SUPPLEMENTARY MATERIAL

Materials and Methods

Immunohistochemistry

For immunohistochemical staining (except for CD34, as noted below), paraffin sections were dewaxed and antigens were retrieved by immersing slides in 0.4 mg/ml proteinase K ready-to-use (Dako, Carpinteria, CA) for 6 min at room temperature for anti-filaggrin, or in 10 mM sodium citrate (pH 6.0) and then autoclaved for anti-TRAP220, anti-Ki67, anti-keratin 1 (K1), anti-keratin 6 (K6), anti-keratin 15 (K15) and anti-SOX9, or were microwaved for anti-filaggrin. After washing in TBS-T, they were treated with H_2O_2 to block endogenous peroxidase activity. After further washing, slides were blocked with Protein Block Serum-Free (Dako), stained with anti-filaggrin (M-290) (1:100; Santa Cruz Biotechnology), anti-Ki67 antigen (polyclonal) (1:500; Leica Microsystems), anti-mouse K1 (AF109) (1:100; Covance) or anti-mouse K6 (1:500; Covance) followed by incubation and visualization with ChemMate ENVISION kit/ HRP (Dako). For MED1 immunostaining, sections were stained with anti-TRAP220 (C-19) (1:200; Santa Cruz Biotechnology) followed by incubation with Biotinylated Link Universal (K0678) (Dako) and then by incubation with HRP-conjugated streptavidin (Dako), and visualization with diaminobenzidine. For K15 immunostaining, slides were stained with anti-mouse K15 (1:10000; Covance) followed by incubation with HRP conjugated anti-chicken IgY (1:500; Promega, Madison, WI), and visualization with diaminobenzidine. For CD34 immunostaining, frozen sections were fixed in acetone, treated with H_2O_2, blocked with Protein Block Serum-Free and stained with anti-CD34 (RAM34) (1:200; BD Biosciences) followed by incubation with biotinylated polyclonal rabbit anti-rat

immunoglobulins (1:300; Dako) and then with streptavidin/HRP (1:300; Dako), and were visualized with diaminobenzidine. Hematoxylin counterstaining was used for K1, K15, filaggrin and CD34 staining. For anti-SOX9 immunostatining, after blocking, slides were stained with anti-SOX9 (KO608) (1:50; Trans Genic, Kobe, Japan) followed by incubation with Alexa Fluor 488 Goat Anti-rabbit IgG (1:500; Molecular Probes, Eugene, OR).

To calculate the ratio of Ki67-positive keratinocytes in *Med1*$^{epi-/-}$ IFE compared to WT, the number of Ki67-positive cells in at least 2 mm length of epidermis in the histological sections from 3 mice for each group were counted, and Student's t test was used for statistical significance.

Calculation of epidermal and dermal thickness, and the diameter of hair shafts.

Histological pictures of H.E. staining were taken using a Biozero BZ-8000 microscope with BZ viewer software (Keyence, Osaka, Japan). The thickness of the epidermis was calculated by measuring the epidermal area over 100 μm horizontal length with BZ analyzer software (Keyence) (Supplementary Figure 2b). Skin specimens from at least 2 mice for each age group of *Med1*$^{epi-/-}$ mice and their WT counterparts were used to calculate epidermal thickness. Three areas for each skin specimen were measured and the average thickness was compared by calculating the relative thickness of *Med1*$^{epi-/-}$ mice. To calculate dermal thickness during the telogen hair cycle, skin specimens derived from three 2-month-old *Med1*$^{epi-/-}$ mice and three WT counterparts were analyzed. Three vertical dermal lengths for each telogen skin specimen were measured on the photographs. To measure the diameter of hair shafts, pelage hairs were plucked by hand from *Med1*$^{epi-/-}$ skin during telogen of the hair cycle at 7 weeks and between 6 to 8 months of age and from their WT counterparts. The diameters of five hair shafts of each hair subtype derived from each mouse were measured at the thickest part on the photographs.

Microarray analysis

Total RNAs were extracted from cultured keratinocytes derived from WT and from *Med1*$^{epi-/-}$ skin using an RNeasy kit (Qiagen, San Diego, CA). Then, 2 μg total RNA was reverse transcribed to cDNA with T7 oligo d(T) primer (Affymetrix, Santa Clara, CA). The cDNA synthesis products were used for in vitro transcription reactions containing T7 RNA polymerase and biotinylated nucleotide analogue (pseudouridine base) cRNAs. The labeled cRNA products were then fragmented and loaded onto GeneChip(R) Mouse Genome 430 2.0 arrays (Affymetrix), and were hybridized according to the manufacturer's protocol. Streptavidin-Phycoerythrin (Molecular Probes) was used as the fluorescent conjugate to detect hybridized target sequences. Raw intensity data from the GeneChip array were analyzed by GeneChip Operating Software (Affymetrix).

	KO/WT >2	ratio (log_2)	KO/WT <1/2	Ratio (log_2)
TGF/ BMP signaling	follistatin-like 1	1.5	TGF beta induced	-2.5
	BMP6	1.2	follistatin	-1.3
IGF/ FGF signaling	FGF7	1.4	IGF2	-1.9
	IGFBP7	1.2	IGFBP4	-1.2
	IGFBP2	1	FGF13	-1.2
			IGF2BP1	-1.1
TNF signaling			TNF alpha induced protein 3	-1.2
cytokines/ secretory protein	Wnt5a	2.4	PDGF	-1.8
	CTGF	1	Wnt10a	-1.5
			IL33	-1.4
			IL24	-1.3
			endothelin 1	-1.1
cytoskelton/ cell adhesion factors	vimentin	1.6	Keratin 75	-1.9
	Tublin beta 2B	1.5	ingegrin beta 6	-1.3
	Keratin 23	1.3	dystrophin	-1.1
	desmoglein 1 beta	1	Claudin 3	-1.1
			myosin heavy polypeptide 9	-1
protease/ protease inhibitor	secretory leukocyte peptidase inhibitor	3.3	kallikrein related peptidase 6	-1.7
	MMP3	3.1	MMP9	-1.3
	TIMP2	2.2		
	ADAM12	1.8		
retinoic acid metabolism	cellular retinoic acid binding protein 1	1.7	retinoid dehydrogenase 9	-1
	aldehyde dehydrogenase 1A3	1.4		
	retinol dehydrogenase 10	1		
transcription factors/ coactivators	Cited2	2	Runx1	-1.2
	Jundm2	1.7	SOX21	-1.1
			trp 63	-1
			SOX9	-1
extracellular matrix protein/ basement membrane protein	extracellular matrix protein 1	1.9	laminin gamma 1	-1
	fibronectin	1.3		
cell surface protein	IL1R2	2	CD109	-1.7
	kit	1.6	Syndecan 4	-1.6
	Syndecan binding protein 2	1.5	Slamf9	-1.2
			ICAM1	-1.1
cell cycle regulation/ apoptosis/ cell fate decision	S100a8	1.9	S100a3	-2
	S100a9	1.7	Gadd45 gamma	-1.5
	cyclin G2	1	Notch1	-1.1
	Bnip3l	1		
	Nupr1	1.1		
microbicidal peptide	defensin beta 3	1.3	defensin beta 1	-2.1
intracellular signaling	G protein signaling modulator	2.2		
	protein kinase C	1.3		
	Ddit4	1.1		
	Ddit3	1		

Supplementary Table

Supplementary Table: Transcriptional profiling of *Med1*$^{epi-/-}$ keratinocytes relative to WT keratinocytes. Microarrays were used to analyze gene expression patterns between keratinocytes derived from *Med1*$^{epi-/-}$ and from WT mice. Functional classifications are shown for the listed genes. The -fold increase for each gene is presented as logarithm to the base 2.

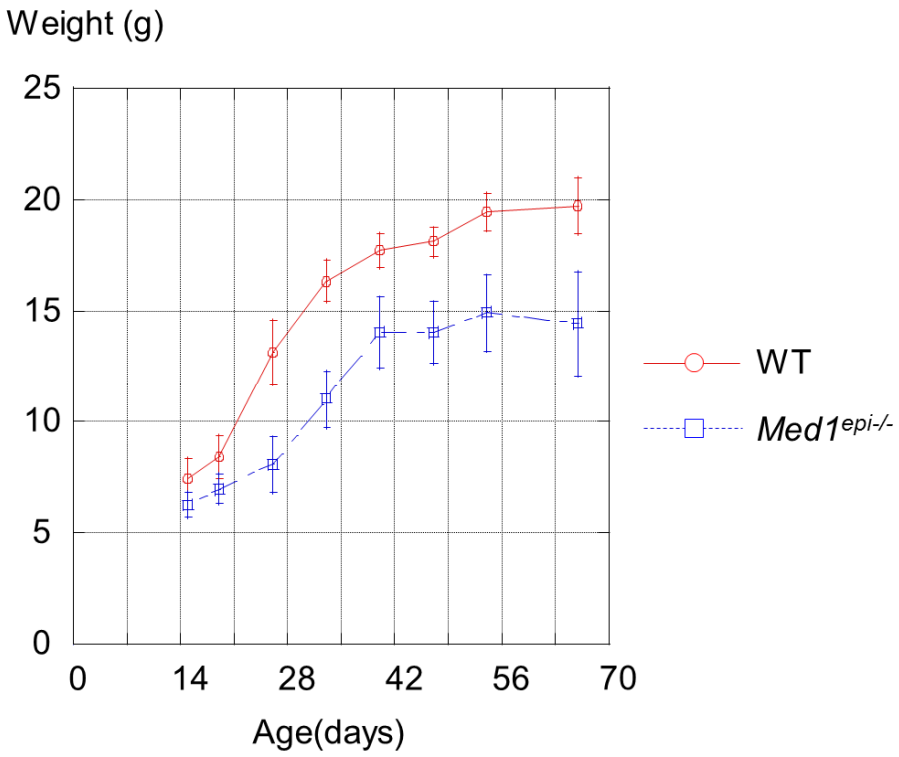

Supplementary Figure 1: Growth retardation of *Med1*$^{epi-/-}$ mice. Representative growth curves of female WT and *Med1*$^{epi-/-}$ mice are presented, indicating the growth retardation of *Med1*$^{epi-/-}$ mice. The average weight of 1-year-old male *Med1*$^{epi-/-}$ mice was 25.6 ± 4.9 g (mean ± s.d.: n=4), and was significantly smaller than WT siblings (44.3 ± 1.4 g: n=3).

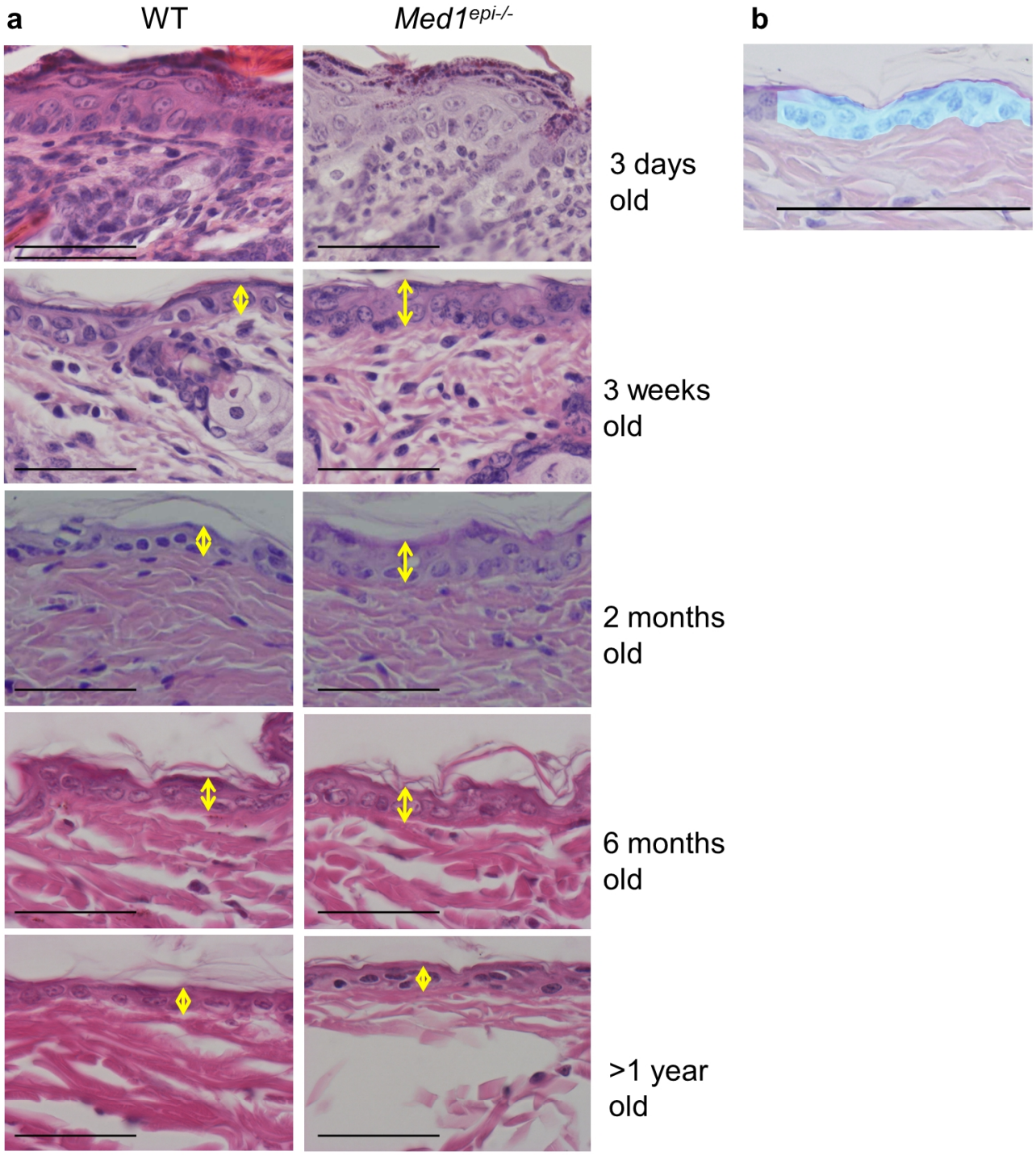

Supplementary Figure 2: **Histological analysis of the IFE in *Med1*$^{epi-/-}$ mice.** (**a**): Skin biopsy specimens taken from WT mice and from *Med1*$^{epi-/-}$ mice at the indicated time points are shown (H.E. staining). The thickness of the IFE is demonstrated by arrows. The IFE of *Med1*$^{epi-/-}$ mice from 3 weeks to 6 months of ages was thicker in these sections. Bar= 50µm. (**b**): The thickness of the epidermis was calculated by measuring the epidermal area over 100 µm in H.E. sections (highlighted area). Bar= 100µm.

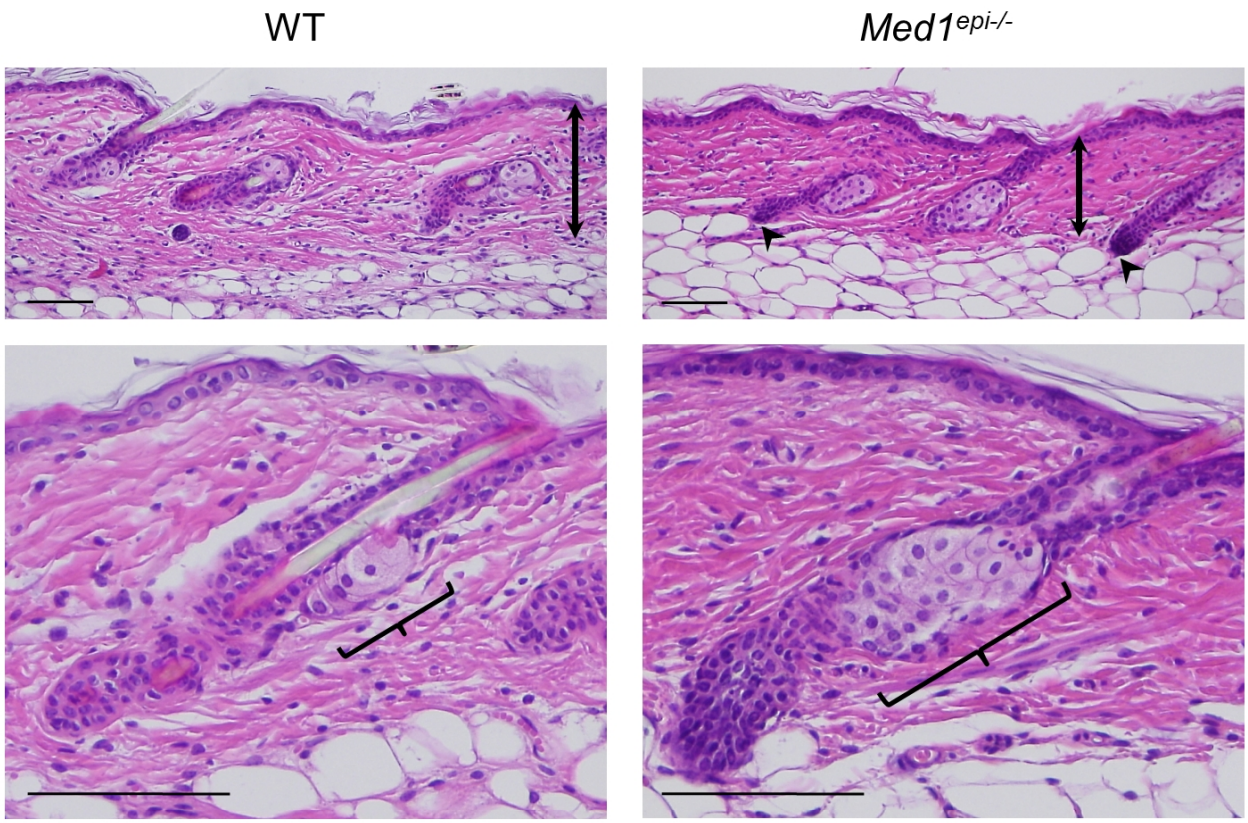

Supplementary Figure 3: **Histological analysis of the dermis and skin appendages in *Med1*$^{epi-/-}$ mice.** Skin biopsy specimens taken from 2-month-old *Med1*$^{epi-/-}$ mice and from their WT counterparts during telogen shows that the dermis is thinner than in WT mice (upper panels). Arrows indicate the thickness of the dermis. The relative dermal thickness of 2-month-old *Med1*$^{epi-/-}$ mice is 0.784 compared to WT mice (n=3, $p<0.01$). Although all telogen WT hair bulbs are in the dermis, some dermal papillae of the *Med1*$^{epi-/-}$ telogen hair follicles are directly in contact with subcutaneous fat (arrowheads). The SG is apparently hyperplastic in the skin of 2-month-old *Med1*$^{epi-/-}$ mice (lower panels; brackets). Bar= 100µm.

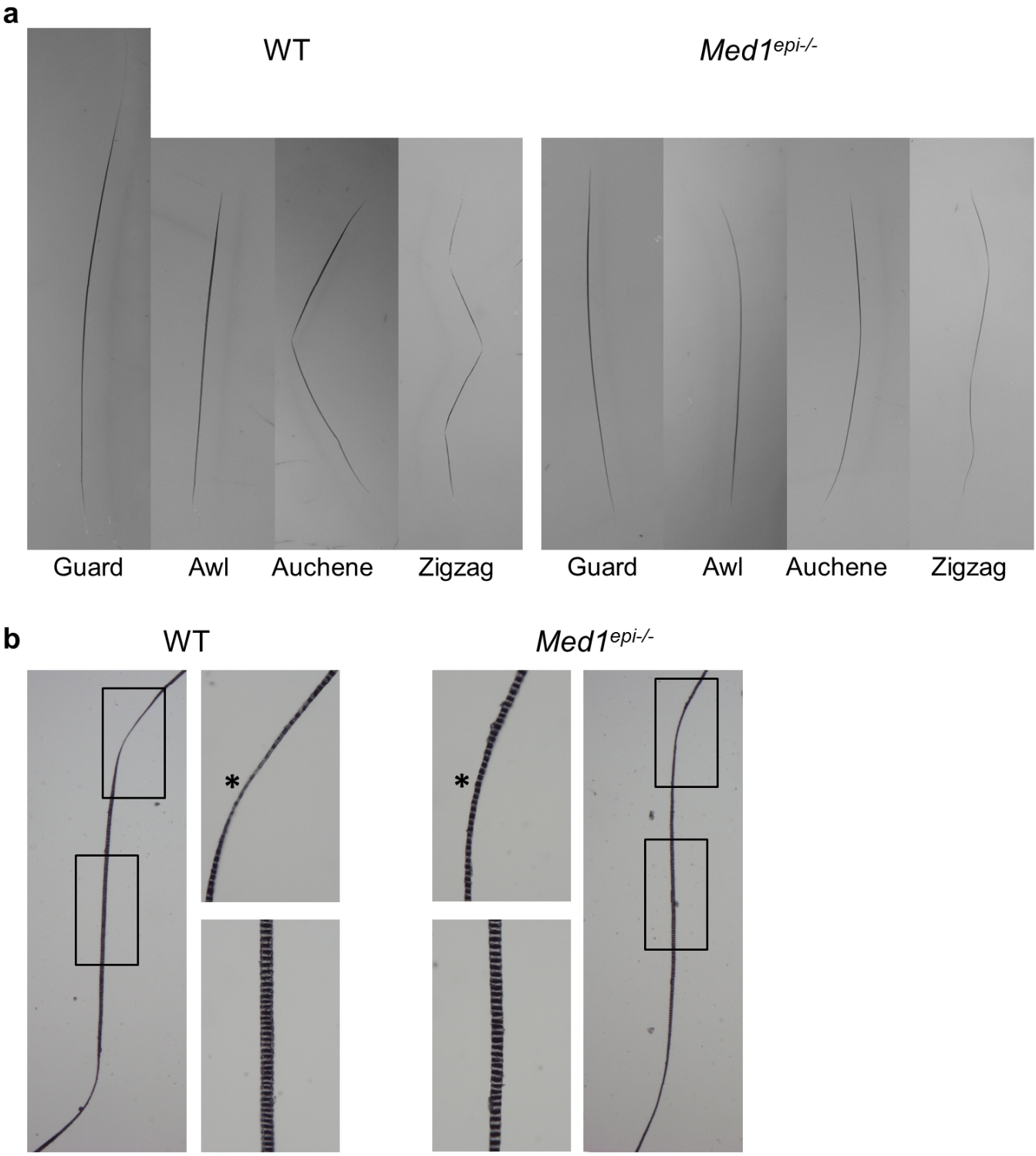

Supplementary Figure 4: Pelage hair structure of *Med1*$^{epi-/-}$ mice was analyzed by microscopy. Hairs were plucked by hand from adult mice and the structure of each hair was analyzed by microscopy. (**a**): Less prominent bends and constrictions in the auchene and zigzag hair types of *Med1*$^{epi-/-}$ mice are observed. (**b**): Microscopic observation of zigzag hairs. The parts enclosed by rectangles are shown in the higher power view. The hair shafts of *Med1*$^{epi-/-}$ mice were smaller than the WT hair shafts. Bending of *Med1*$^{epi-/-}$ zigzag hairs tended to be smaller. The average internal angle of WT zigzag hair was $129.8 \pm 14.9^{\circ}$, while that of *Med1*$^{epi-/-}$ was $136.1 \pm 10.9^{\circ}$; the average difference is not statistically significant by Student's t test (n=4, p=0.14). The distance between the pigmented bands is shorter in the bending part of hairs from *Med1*$^{epi-/-}$ mice (asterisks).

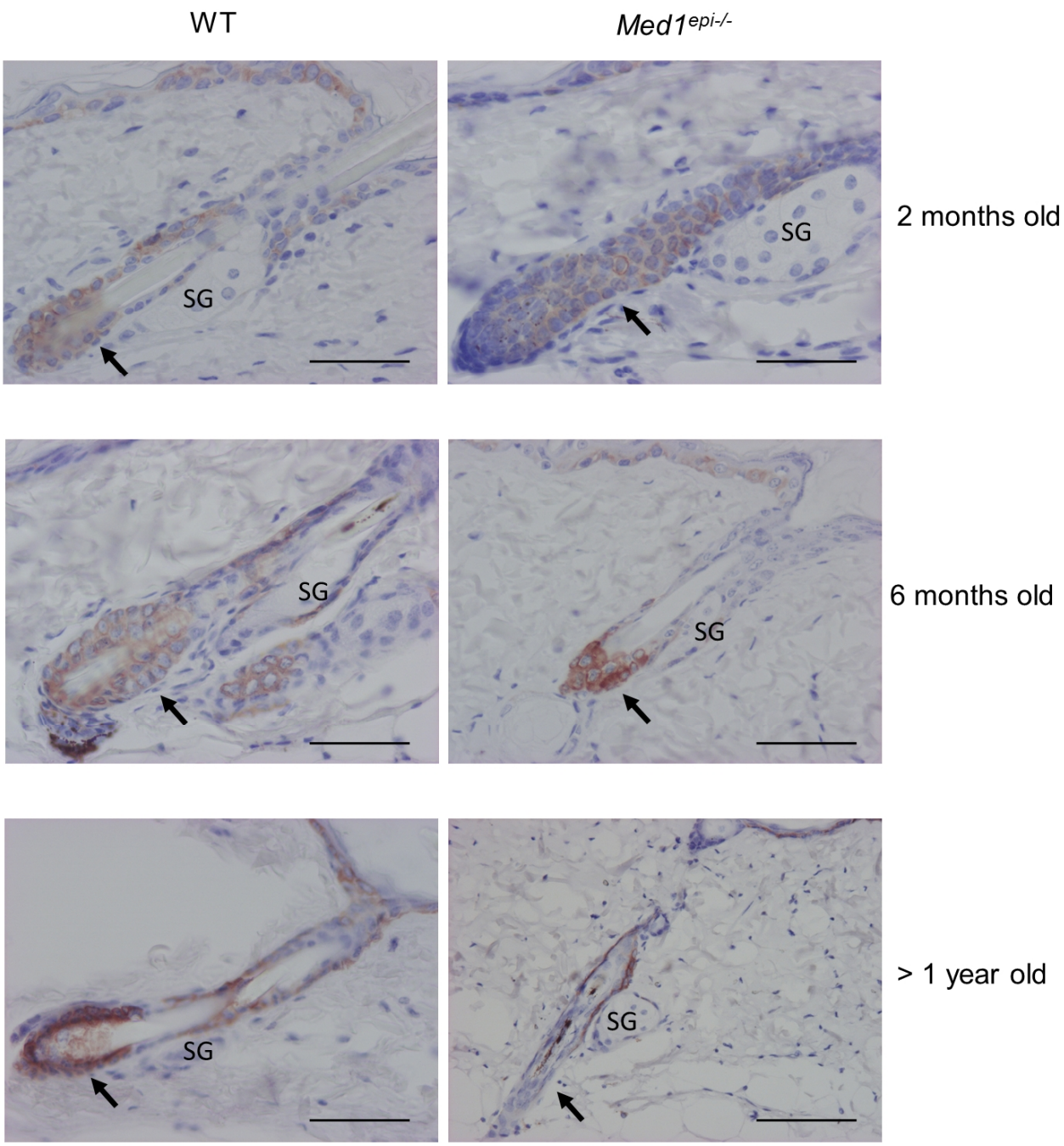

Supplementary Figure 5: K15-positive bulge cells are decreased in aged *Med1*$^{epi-/-}$ hair follicles. Immunohistochemical staining shows K15-positive cells in *Med1*$^{epi-/-}$ and WT hair follicles at the indicated time points. In contrast to bulge cells in WT hair follicles that are stained with K15 at all time points, those in *Med1*$^{epi-/-}$ hair follicles are not stained with K15 after 1 year of age. Bulge cells are indicated by arrows. Bar= 100µm.

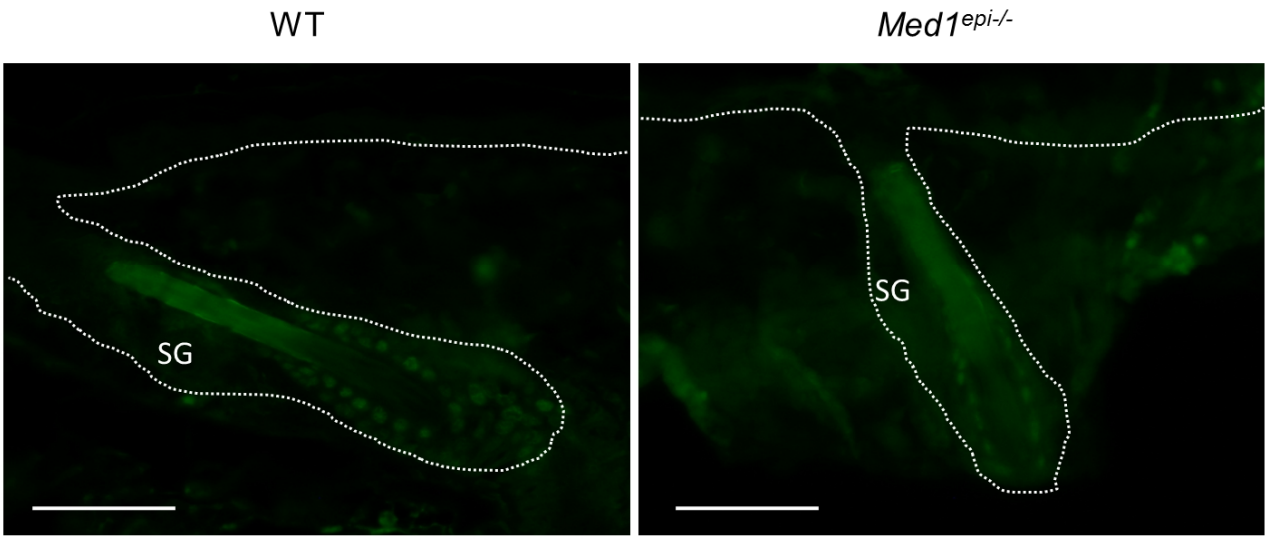

Supplementary Figure 6: Decreased expression of SOX9 in the bulge of *Med1*$^{epi-/-}$ hair follicles. Immunohistochemical staining shows SOX9-positive staining in 6-month-old *Med1*$^{epi-/-}$ and WT hair follicles. Comparing with strong nuclear staining in the WT bulge, bulge cells of some *Med1*$^{epi-/-}$ hair follicles are weakly stained with anti-SOX9 antibody. Bar= 100μm.